Letter Vol. 44, No. 7 / 1 April 2019 / Optics Letters 1611

Ring-core photonic crystal fiber for propagation of OAM modes

Arsène Tandjè,[1,2] Jean Yammine,[1] Michel Dossou,[2] Géraud Bouwmans,[1] Karen Baudelle,[1] Antoine Vianou,[2] Esben Ravn Andresen,[1] and Laurent Bigot[1,*]

[1]Université de Lille, CNRS, UMR 8523—PhLAM—Physique des Lasers Atomes et Molécules, F-59000 Lille, France
[2]Polytechnic School of Abomey-Calavi (EPAC), University of Abomey-Calavi (UAC), Cotonou, Benin
*Corresponding author: laurent.bigot@univ-lille.fr

Received 17 December 2018; revised 6 February 2019; accepted 24 February 2019; posted 25 February 2019 (Doc. ID 355553); published 21 March 2019

We propose and fabricate a novel ring-core photonic crystal fiber made of a circular ring core surrounded by a cladding constituted of air holes organized in a first circular ring surrounded by hexagonal ones. The fiber efficiently supports four different groups of orbital angular momentum (OAM) modes. The effective indices of spin-orbit aligned and spin-orbit anti-aligned modes in the same OAM modes group are separated by at least 2.13×10^{-3} at 1550 nm. The realized fiber is expected to be a good platform for applications involving OAM modes.

https://doi.org/10.1364/OL.44.001611

It is known that some light beams possess angular momentum and that this angular momentum can be separated into a spin angular momentum (SAM) and an orbital angular momentum (OAM) [1]. Today there is a strong interest for this light property, since it is used in optical tweezers to drive micro-machines by angular momentum transfer, atomic selection, nonlinear interactions, or mode-division multiplexing (MDM) [2–5]. The SAM is related to the polarization of light, whereas OAM refers to a helical phase dependence of the electric field. In cylindrical optical fiber, OAM modes are obtained by linear combinations of vector modes: $\mathrm{OAM}^{\pm}_{\pm lm} = \mathrm{HE}^{\mathrm{even}}_{(l+1)m} \pm j\mathrm{HE}^{\mathrm{odd}}_{(l+1)m}$ (for $l \geq 0$) and $\mathrm{OAM}^{\mp}_{\pm lm} = \mathrm{EH}^{\mathrm{even}}_{(l-1)m} \pm j\mathrm{EH}^{\mathrm{odd}}_{(l-1)m}$ (for $l > 1$) [6]. Then the HE vector modes give rise to OAM modes with the spin and orbital momentum aligned, while the EH vector modes give rise to OAM modes with anti-aligned spin and orbital momentum. Note that $\mathrm{OAM}^{\pm}_{01}$ is circularly polarized and has no topological charge. The vector modes TE_{0m} and TM_{0m} are two other types of vector modes that permit us to construct OAM modes with topological charge $|l| = 1$: $\mathrm{OAM}^{\mp}_{\pm 1m} = \mathrm{TM}_{0m} \pm \mathrm{TE}_{0m}$. However, TE and TM vector modes have different propagation constants; then the resulting OAM modes are not propagation-invariant [7]. This is not the case for the odd and even components of each hybrid mode which, in a circular fiber, have exactly the same effective index (n_{eff}) and, then, unlike linearly polarized $\mathrm{LP}_{l,m}$ modes with $l \neq 0$, OAM modes do not present mode beating during propagation (the beat length being defined by $L_{\mathrm{beat}} = \lambda/\Delta n_{\mathrm{eff}}$, where Δn_{eff} is the effective index difference between the two modes that are considered). Since several OAM modes can coexist simultaneously in an optical fiber and considering that these modes can provide limited coupling between them, they potentially constitute a set of nearly independent pathways in the context of data multiplexing over modes [3,4]. Today MDM is performed with both LP and OAM modes. It has been shown that it is possible to use the four states of an OAM_{lm} mode family to perform multiple-input multiple-output (MIMO)-free transmission [8]. In the worst case, a 2×2 MIMO data processing will be necessary, as is used today in coherent optical fiber communications where signal is encoded on the two polarization states of the fundamental mode of a single-mode fiber. As a point of comparison, a 4×4 MIMO processing is necessary if one uses the four states of a LP_{lm} mode ($l \geq 1$) in an optical fiber with circular symmetry. Since $N \times N$ MIMO scales in complexity with N^2 [9], one can prefer OAM modes for MDM communications systems. In order to minimize coupling between OAM modes, a minimum Δn_{eff} of 10^{-4} is generally targeted between $\mathrm{HE}_{(l+1)m}$ and $\mathrm{EH}_{(l-1)m}$ modes [10]. Ring-core geometry is well adapted to the guidance of OAM modes, since it can eliminate the undesirable modes $m = 2$ and reach a large enough intra-mode-group OAM Δn_{eff} value if a high-index contrast is achieved. In fact, avoiding higher-order OAM modes ($m \geq 2$) simplifies the multiplexing and the demultiplexing of modes, because all the OAM modes present an annular intensity shape [11]. Since a vortex fiber was used for terabit-scale data transmission by MDM, including OAM^{+}_{11} and OAM^{-}_{-11}, which were separated from TE and TM modes by $\Delta n_{\mathrm{eff}} \approx 1.6 \times 10^{-3}$ [4], many other fibers have been designed so as to increase the number of supported OAM modes and minimize mode coupling. To reach this goal, it is necessary to realize large index differences (Δn) between the ring core and its adjacent layers. Nevertheless, using conventional techniques such as the modified chemical vapor deposition, it is quite difficult to reach high Δn in a silica optical fiber made of conventional co-doping such as germanium and fluorine. Up to now, index contrasts less than 45×10^{-3} were reported in step index fibers [4,11–13]

and graded-index ones [14]. Moreover, the minimum intra-mode-group OAM Δn_{eff} value generally decreases as the number of supported modes increases for a given Δn. Although high index contrast could be achieved with air-silica photonic crystal fibers (PCFs), OAM-dedicated PCFs have not been realized yet, and OAM with $|l| = 1$ guidance in a PCF has only been reported in twisted PCFs [15]. Hence, it is the aim of this Letter to experimentally evaluate the potential of a new ring-core PCF designed for the guidance of OAM modes with low mode coupling. This Letter is organized as follows: first, the possibilities and limitations of the ring-core PCFs with hexagonal symmetry will be discussed; then, a modified PCF design which retains the properties of OAM will be proposed and manufactured; finally, the fabricated PCF will be characterized.

PCFs are usually manufactured by the stack-and-draw method for which hexagonal symmetry respects the natural arrangement of capillaries. However, when adapted to ring-core configuration, this geometry is not very suitable for the guidance of stable OAM modes, whereas high-index contrast can be achieved between the core and the cladding. This is illustrated by Fig. 1 which presents a ring-core photonic crystal fiber with hexagonal symmetry and shows that HE_{41}^{even} and EH_{21}^{even} modes are degenerate, as well as HE_{41}^{odd} and EH_{21}^{odd} modes. At the same time, one can note that the degeneracy between even and odd modes can also be lifted (in Fig. 1, HE_{31}^{even} and HE_{31}^{odd} present a Δn_{eff} value about 2.8×10^{-3}). For OAM modes, the invariance in propagation and weak coupling, hence, seems difficult to achieve in such a geometry. This explains why some designs of circular air-silica ring-core PCFs have been theoretically proposed in the literature [16–18]. Those designs show a large Δn_{eff} value between $HE_{(l+1)1}$ and $EH_{(l-1)1}$ ($>4.3 \times 10^{-4}$ [17]). Figure 2 illustrates the case of a circular ring-core PCF with a maximum degeneracy lifting between even and odd modes of 2.5×10^{-5}. Thanks to that arrangement, the Δn_{eff} between the even and odd modes can be strongly reduced in contrast to the hexagonal arrangement in Fig. 1. However, it appears that such a geometry is not easy to manufacture by stack-and-draw due to a nonuniform pitch (hole-to-hole distance) in the different rings of the micro-structured cladding. Several attempts to produce such fiber structures have been carried out in our group without success. An alternative structure has hence been considered.

The proposed structure consists in a solid ring-core sandwiched between a central hole and a circular ring of air holes. The cladding structure is then prolongated by several rings of air holes with hexagonal symmetry. In practice, the circular ring

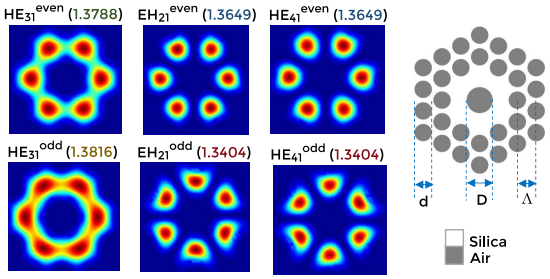

Fig. 1. (Left): transverse intensities and n_{eff} of selected vector modes at 1.55 μm of (right) a studied hexagonal PCF with $d = 1.6$ μm, $D = 2.4$ μm, and $\Lambda = 2$ μm.

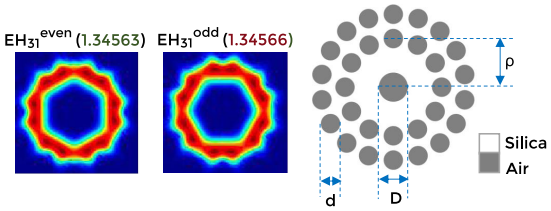

Fig. 2. (Left): transverse intensities and n_{eff} of EH_{31}^{even} and EH_{31}^{odd} modes at 1.55 μm of (right) a circular PCF with $d = 1.6$ μm, $D = 2.4$ μm, and $\rho = 4$ μm.

makes it possible to obtain a close-to-circular symmetry favorable for the propagation-invariant OAM modes. The three additional rings, used to increase light confinement in the ring core, possess a hexagonal symmetry, more easy to manufacture by the stack-and-draw method (Fig. 3).

In order to maximize the number of guided modes and intra-mode-group OAM Δn_{eff} value, the following geometry was chosen for the designed ring-core PCF: the central air hole has a diameter $D = 5.4$ μm, and the first ring of the holey cladding is made air holes of diameter $d_C = 2.6$ μm arranged circularly with a curvature radius $\rho = 5.4$ μm. We defined their number as 12 to easily match the circular ring to the following hexagonal ring. The spatial positions of the air holes on the first ring in the (Ox, Oy) plane are then given by

$$x = \rho \cos\left(\frac{\pi n}{6}\right), \qquad y = \rho \sin\left(\frac{\pi n}{6}\right), \qquad n = 1 \text{ to } 12. \quad \textbf{(1)}$$

The hexagonal outer rings are made of air holes of diameter $d_H = 2.9$ μm, together with a pitch $\Lambda_H = 3.0$ μm. The background material is made of pure silica. The guiding region is annular-like and located between the central air hole and the first circular ring. The silica ring is thin enough (~1.4 μm) to avoid the existence of modes with $m = 2$ and to reach a good separation of the effective indices between modes:

$$P_l = \frac{\left|\iint \exp(-j \times \text{Arg}(E_l)) \times \exp(-jl\varphi) dA\right|^2}{\iint |\exp(j \times \text{Arg}(E_l))|^2 dA \times \iint |\exp(-jl\varphi)|^2 dA}. \quad \textbf{(2)}$$

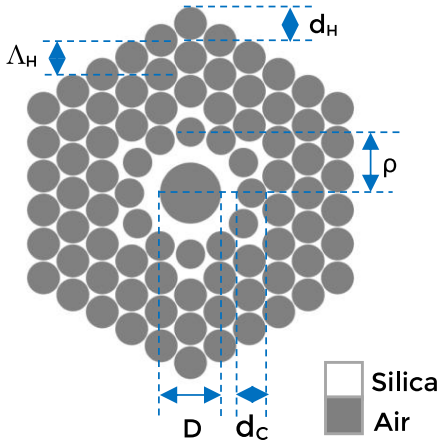

Fig. 3. Cross section and main parameters of the proposed ring-core PCF geometry.

The designed ring-core PCF has been theoretically studied using COMSOL Multiphysics to determine its modal properties. The intensity profiles of the first 10 vector modes are displayed in Fig. 4. We also calculated the intensities and the phases of the guided OAM modes of the fiber. We evaluated the purity P_l of each OAM state phase using the overlap integral between $\exp(j \times \mathrm{Arg}(E_l))$ and $\exp(-jl\varphi)$ (relation 2), where $\mathrm{Arg}(E_l)$ is the argument of the electric field E_l of a guided mode with topological charge l. For example, we reported in Fig. 5 the intensities of OAM_{11}^{+} and OAM_{41}^{+} modes. It can be seen that they have an annular shape and that their phases show the expected topological charge with a purity more than 94%. This new design allowed us to limit the degeneracy lifting to less than 2.7×10^{-8} between the even and odd modes (due to the size of the air-holes). The $\mathrm{HE}_{(l+1)1}$ and $\mathrm{EH}_{(l-1)1}$ modes are very well separated in terms of n_{eff} values at 1.55 μm. Table 1 presents, in descending order, the effective index of the different guided modes, as well as Δn_{eff} between two successive vector modes. The smallest value is 7.24×10^{-4} and is between TE_{01} and HE_{11} modes. Such a large value had not yet been achieved in an OAM fiber guiding so many modes. It can be expected that all the modes of this fiber can be used with a potentially low inter-modal coupling (including the fundamental mode HE_{11}). Note that the smallest effective index difference between spin-orbit aligned and spin-orbit anti-aligned OAM modes belonging to the same group (same $|l|$) is as high as 2.13×10^{3}, well beyond the minimum value of 10^{-4}, generally targeted to ensure a very weak coupling between these modes [10].

Simulations have been performed over a wide wavelength range of 750 nm. Figure 6 shows the effective indices of the vector modes of the fiber as a function of the wavelength from 1250 to 2000 nm. It can be seen that all the modes are well separated over the entire bandwidth, and the separation increases with the wavelength. Besides the fact that the potential interest is for applications in the C-band, the fiber could then be used in different telecommunication windows, because it shows a good mode separation for these wavelengths.

Confinement losses (CLs) have also been calculated. Indeed, over the entire wavelength range (from 1250 to 2000 nm), due to a large d/Λ ratio, CLs are negligible, the largest calculated value being about 2×10^{-5} dB km^{-1} for the 10 vector modes. Note that, in the current design, $2d_C/\rho$ is about 0.96, and d_H/Λ_H is close to 0.96.

The proposed fiber has been fabricated using the stack-and-draw approach. Capillaries and rods with appropriate dimensions have been drawn, assembled, and inserted into a tube. This preform has then been drawn into a cane and, after sleeving into a second tube, drawn into a fiber. The scanning electron microscope (SEM) picture of the whole fiber structure is presented in Fig. 7, together with a zoom on the ring-core. The obtained fiber has a geometry quite close to the targeted design. More precisely, $D \sim 5.26$ μm, $d_C \sim 2.61$ μm, $\rho \sim 5.30$ μm, $d_H \sim 2.87$ μm, and $\Lambda_H \sim 3.09$ μm.

The total losses over a wide wavelength range from 800 to 1700 nm were measured by the cut-back method using

Table 1. Vector Modes, OAM Group, n_{eff}, and Δn_{eff}, Between Adjacent Vector Modes in Designed Ring-Core PCF at 1.55 μm

Modes	$\lvert l\rvert$	n_{eff}	Δn_{eff} (1×10^{3})
TE_{01}	1	1.391767	
HE_{11}	0	1.391043	0.724
HE_{21}	1	1.388116	2.93
HE_{31}	2	1.382111	6.01
TM_{01}	1	1.380336	1.77
EH_{11}	2	1.377453	2.88
HE_{41}	3	1.372699	4.75
EH_{21}	3	1.369591	3.11
HE_{51}	4	1.359903	9.69
EH_{31}	4	1.357772	2.13

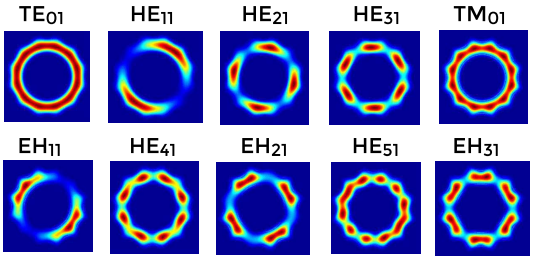

Fig. 4. Simulation of guided vector modes at 1.55 μm of the proposed ring-core PCF.

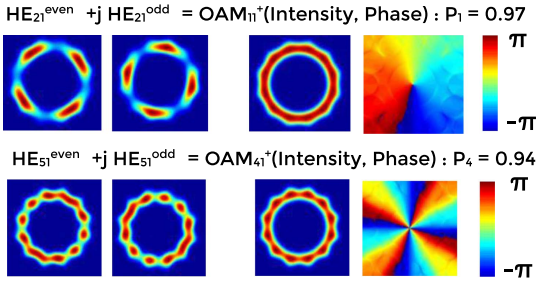

Fig. 5. Intensities, phases, and purities of calculated OAM_{11}^{+} and OAM_{41}^{+} modes at 1.55 μm supported by the proposed ring-core PCF.

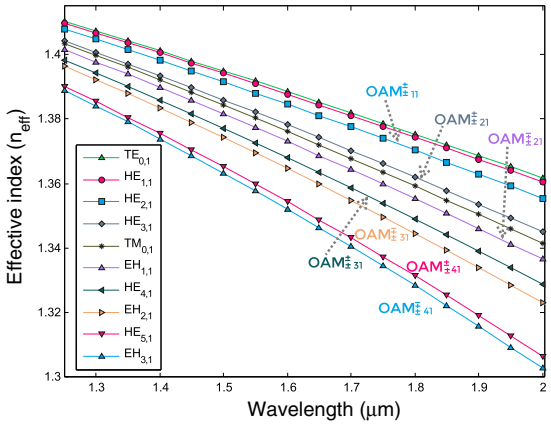

Fig. 6. Effective index of the vector modes guided by the proposed ring-core PCF as a function of the wavelength.

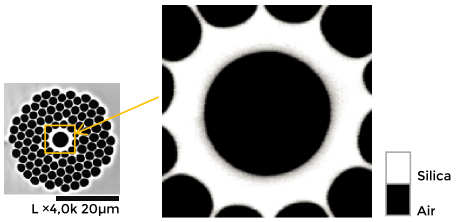

Fig. 7. SEM image of the fabricated ring-core PCF.

100 and 2 m lengths of the fiber rolled on a 15.8 cm diameter spool (Fig. 8). The global losses at 1550 nm were around 50 dBkm^{-1}. Therefore, the fiber can be tested over distances of about 100 m.

The guidance of OAM modes has then been analyzed. Using a spatial light modulator (SLM), a free-space Gaussian beam has been converted into an OAM beam with topological charge l by displaying a phase mask $\varphi(\rho,\theta) = l \times \theta$ on the SLM, where (ρ,θ) are the radial and azimuthal coordinates on the SLM centered on the incoming Gaussian beam. The polarization state of the free-space OAM beams has been converted to circular and coupled into the ring-core PCF using a ×40 and 0.65 NA microscope objective, exciting the OAM modes of the fiber with the same topological charge. A dedicated setup then permitted to analyze the interference between the light emerging from the other end of 1.2 m of the ring-core PCF and a plane wave used as reference. The results of this interference are presented in Fig. 9 (right). The "fork-like" pattern in the

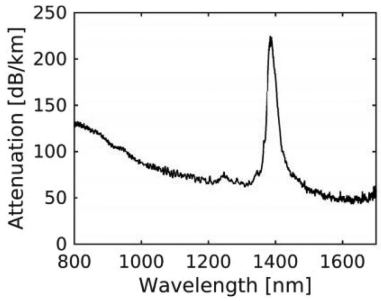

Fig. 8. Global losses of the fabricated ring-core PCF.

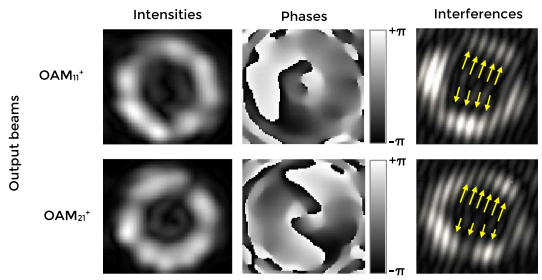

Fig. 9. Measured CCD images of OAM with $l = 1$ (top) and $l = 2$ (bottom) output signals of a ring-core PCF: (left) intensities, center (phases), and (right) interferences with a plane wave.

interference fringes indicates the presence of the expected topological charges, also confirming the propagation of right circularly polarized OAM modes with $l = 1$ and 2. Off-axis holographic processing make it possible to extract the phase and intensity of guided OAM modes from an image recorded with a CCD camera. Figure 9 (left) and (center) show the results for OAM modes with $l = 1$ and 2.

We have designed a new ring-core PCF that supports up to four OAM mode groups. The proposed design makes it possible to efficiently lift the degeneracy between the guided $HE_{(l+1)1}$ and $EH_{(l-1)1}$ modes and a minimum difference of the effective indices of 2.13×10^3 is predicted at 1550 nm. The fiber was fabricated and preliminary characterizations have been performed and presented as a proof of concept. Work is in progress to improve the regularity of the structure and the background losses so as to fully exploit the potential offered by such fibers.

Funding. IRCICA Institute, USR CNRS 3380 of University of Lille; Labex CEMPI (ANR-11-LABX-0007); Equipex FLUX (ANR-11-EQPX-0017); French Ministry of Higher Education and Research and the "Hauts de France" Régional Council through the CPER "Photonics for Society."

Acknowledgment. The fiber was made at FiberTech Lille (http://fibertech.univ-lille.fr).

REFERENCES

1. M. W. B. Allen, Phys. Rev. A **45**, 8185 (1992).
2. A. M. Yao and M. J. Padgett, Adv. Opt. Photonics **3**, 161 (2011).
3. A. E. Willner, H. Huang, Y. Yan, Y. Ren, N. Ahmed, G. Xie, C. Bao, L. Li, Y. Cao, Z. Zhao, J. Wang, M. P. J. Lavery, M. Tur, S. Ramachandran, A. F. Molisch, N. Ashrafi, and S. Ashrafi, Adv. Opt. Photonics **7**, 66 (2015).
4. N. Bozinovic, Y. Yue, Y. Ren, M. Tur, P. Kristensen, H. Huang, A. E. Willner, and S. Ramachandran, Science **340**, 1545 (2013).
5. G. Li, N. Bai, N. Zhao, and C. Xia, Adv. Opt. Photonics **6**, 413 (2014).
6. S. Ramachandran and P. Kristensen, Nanophotonics **2**, 455 (2013).
7. C. Brunet and L. A. Rusch, Opt. Fiber Technol. **31**, 172 (2016).
8. K. Ingerslev, P. Gregg, M. Galili, F. D. Ros, H. Hu, F. Bao, M. A. U. Castaneda, P. Kristensen, A. Rubano, L. Marrucci, K. Rottwitt, T. Morioka, S. Ramachandran, and L. K. Oxenløwe, Opt. Express **26**, 20225 (2018).
9. N. K. Fontaine, R. Ryf, H. Chen, A. V. Benitez, B. Guan, R. Scott, B. Ercan, S. J. B. Yoo, L. E. Grüner-Nielsen, Y. Sun, R. Lingle, E. Antonio-Lopez, and R. Amezcua-Correa, in *Optical Fiber Communication Conference Post Deadline Papers* (OSA, 2015), p. Th5C.1.
10. S. Ramachandran, P. Kristensen, and M. F. Yan, Opt. Lett. **34**, 2525 (2009).
11. C. Brunet, P. Vaity, Y. Messaddeq, S. LaRochelle, and L. A. Rusch, Opt. Express **22**, 26117 (2014).
12. P. Gregg, P. Kristensen, and S. Ramachandran, Opt. Express **24**, 18938 (2016).
13. X. Wang and Y. Song, Opt. Express **25**, 29342 (2017).
14. B. Ung, P. Vaity, L. Wang, Y. Messaddeq, L. A. Rusch, and S. LaRochelle, Opt. Express **22**, 18044 (2014).
15. X. M. Xi, G. K. L. Wong, M. H. Frosz, F. Babic, G. Ahmed, X. Jiang, T. G. Euser, and P. St.J. Russell, Optica **1**, 165 (2014).
16. H. Zhang, W. Zhang, L. Xi, X. Tang, W. Tian, X. Zhang, and X. Zhang, in *Asia Communications and Photonics Conference* (Optical Society of America, 2015), pp. ASu2A-54.
17. H. Zhang, W. Zhang, L. Xi, X. Tang, X. Zhang, and X. Zhang, IEEE Photonics Technol. Lett. **28**, 1426 (2016).
18. H. Zhang, X. Zhang, H. Li, Y. Deng, X. Zhang, L. Xi, X. Tang, and W. Zhang, Opt. Commun. **397**, 59 (2017).